Chemistry & Biology
Article

# Characterization of Monoacylglycerol Lipase Inhibition Reveals Differences in Central and Peripheral Endocannabinoid Metabolism

Jonathan Z. Long,[1] Daniel K. Nomura,[1] and Benjamin F. Cravatt[1,*]
[1]The Skaggs Institute for Chemical Biology and Department of Chemical Physiology, The Scripps Research Institute, 10550 N. Torrey Pines Rd. La Jolla, CA 92037, USA
*Correspondence: cravatt@scripps.edu
DOI 10.1016/j.chembiol.2009.05.009

## SUMMARY

**Monoacylglycerol lipase (MAGL) is a principal degradative enzyme for the endocannabinoid 2-arachidonoylglycerol (2-AG). We recently reported a piperidine carbamate, JZL184, that inhibits MAGL with high potency and selectivity. Here, we describe a comprehensive mechanistic characterization of JZL184. We provide evidence that JZL184 irreversibly inhibits MAGL via carbamoylation of the enzyme's serine nucleophile. Functional proteomic analysis of mice treated with JZL184 revealed that this inhibitor maintains good selectivity for MAGL across a wide range of central and peripheral tissues. Interestingly, MAGL blockade produced marked, tissue-specific differences in monoglyceride metabolism, with brain showing the most dramatic elevations in 2-AG and peripheral tissues often showing greater changes in other monoglycerides. Collectively, these studies indicate that MAGL exerts tissue-dependent control over endocannabinoid and monoglyceride metabolism and designate JZL184 as a selective tool to characterize the functions of MAGL in vivo.**

## INTRODUCTION

Monoacylglycerol lipase (MAGL) is a 33 kDa, peripherally associated membrane enzyme of the serine hydrolase superfamily that catalyzes the hydrolysis of monoacylglycerols (MAGs) to free fatty acid and glycerol (Karlsson et al., 1997; Tornqvist and Belfrage, 1976). MAGL contains the classical GXSXG consensus sequence common to most serine hydrolases and is predicted by sequence homology to have an $\alpha/\beta$-hydrolase fold. The catalytic triad has been identified as Ser122, His269, and Asp239 (Karlsson et al., 1997). Though MAGL can hydrolyze 1(3)- and 2-MAGs equally efficiently, it has an exquisite substrate preference for MAGs over triacylglycerols and diacylglycerols (Fredrikson et al., 1986; Tornqvist and Belfrage, 1976). Beyond its initially described contribution to lipolysis in adipose tissue, MAGL has also been proposed to degrade the endogenous cannabinoid (endocannabinoid) 2-arachidonoylglycerol (2-AG) (Mechoulam et al., 1995; Sugiura et al., 1995) in the nervous system (Dinh et al., 2002). 2-AG, along with a second endocannabinoid anandamide (AEA) (Devane et al., 1992), are signaling lipids that activate the cannabinoid receptors CB1 (Matsuda et al., 1990) and CB2 (Munro et al., 1993), two G-protein-coupled receptors that also mediate the neurobehavioral and immunosuppressive effects of the psychoactive component of marijuana, $\Delta^9$-tetrahydocannabinol (Ledent et al., 1999; Mackie, 2006; Zimmer et al., 1999). Endocannabinoids have been implicated in the regulation of a number of (patho)physiological processes that reflect functions in both the nervous system (e.g., pain, anxiety, cognition) and peripheral tissues (e.g., dyslipidemia, inflammation, fertility) (Di Marzo et al., 2007; Mackie, 2006).

Endocannabinoid signaling is terminated by enzymatic hydrolysis, a process that, for AEA, occurs by the action of fatty acid amide hydrolase (FAAH) (Cravatt et al., 1996, 2001). Although several enzymes have been implicated in the hydrolysis of 2-AG, we and others have provided evidence that MAGL is the principal 2-AG hydrolase in rodent brain (Blankman et al., 2007; Dinh et al., 2002, 2004; Nomura et al., 2008a, 2008b). To investigate the role that MAGL plays in endocannabinoid metabolism and signaling in vivo, we recently described a potent and selective inhibitor of this enzyme termed JZL184 (Long et al., 2009) that, upon administration to mice, decreased brain MAG hydrolysis activity by up to 85% and dramatically elevated brain 2-AG levels. These biochemical and metabolic changes were accompanied by several CB1-dependent behavioral phenotypes, including hypomotility, hypothermia, and analgesia. Key to the development of JZL184 was the implementation of competitive activity-based protein profiling (ABPP) screens (Leung et al., 2003; Li et al., 2007) to direct the concurrent optimization of inhibitor potency and selectivity. Here, we extend this initial study by presenting a detailed mechanistic characterization of JZL184. We provide evidence that JZL184 inhibits MAGL by carbamoylation of the enzyme's active site serine nucleophile. We also demonstrate that JZL184 can be used to globally inactivate MAGL in both central and peripheral tissues, where the inhibitor maintains good selectivity, showing only a handful of off-targets in a select subset of tissues. Interestingly, we observed marked tissue-specific differences in the accumulation of 2-AG and other MAG species upon MAGL inhibition, suggesting that endocannabinoid tone and its regulation by MAGL vary across individual organs.

## RESULTS

### JZL184 Inhibits MAGL by Irreversible Active-Site Carbamoylation

Carbamate inhibitors typically inactivate serine hydrolases by irreversible (or slowly reversible) covalent modification

 

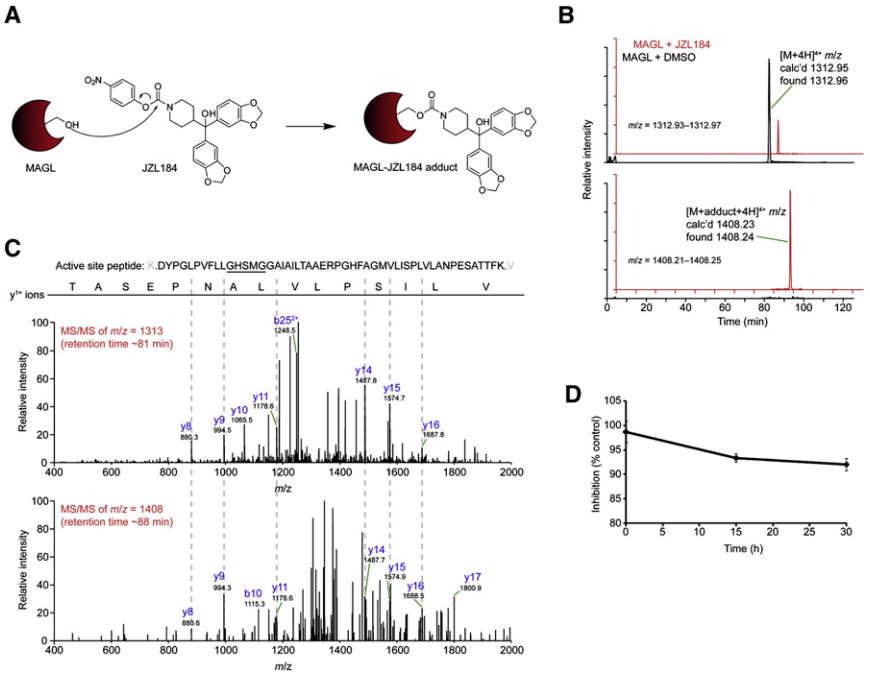


**Figure 1. Mechanism of JZL184 Inhibition of MAGL**

(A) Proposed mechanism for covalent inactivation of MAGL by JZL184 involving carbamoylation of the enzyme's catalytic serine nucleophile (Ser122).

(B) Extracted ion chromatograms (EIC) of the unmodified (top) and JZL184-modified (bottom) MAGL active site tryptic peptide (amino acids 110–160). Recombinant, purified human MAGL was treated with DMSO (black trace) or JZL184 (200 μM, red trace). The mass window for each EIC, the detected high-resolution mass for each peak, and the charge state for each tryptic peptide are indicated.

(C) MS/MS spectra generated by the unmodified and modified active site peptides. Diagnostic y and b ions are identified. All ions are in the 1+ charge state unless otherwise indicated.

(D) JZL184-treated MAGL was incubated at room temperature in 50 mM Tris (pH 8.0), and the activity remaining as a percentage of control reactions (treated with DMSO) was measured by 2-AG hydrolysis assays. Data are presented as mean ± SEM of three independent experiments.

(carbamoylation) of the catalytic serine nucleophile (Alexander and Cravatt, 2005; Bar-On et al., 2002) (Figure 1A). We therefore sought to test whether this mechanism was operational for inhibition of MAGL by JZL184. JZL184-treated and dimethyl sulfoxide (DMSO)-treated (control) preparations of purified MAGL were digested with trypsin and analyzed by liquid chromatography tandem mass spectrometry (LC-MS/MS) on a high-resolution instrument (LTQ-Orbitrap). We searched the resulting MS1 (parent ion) profiles for masses corresponding to the unmodified and carbamoylated forms of the MAGL active site peptide. In control samples without inhibitor, we observed a single peak with $m/z$ = 1312.96, corresponding to the 4+ charge state of the unmodified MAGL active site tryptic peptide, amino acids 110–160. In samples treated with JZL184, a new peak appeared with $m/z$ = 1408.24, corresponding to the 4+ charge state of the carbamoylated form of the active site peptide (Figure 1B). The detected adduct was unique to the active site peptide, because an analysis of other tryptic peptides derived from MAGL revealed no evidence of JZL184 adducts (see Figure S1 available online). MS/MS analysis of the unmodified and JZL184-modified forms of the active site peptide identified six common $y^{1+}$ fragment ions (Figure 1C). Notably, the active site peptide contains three serine residues, and two of these serines are detected in unmodified form in the $y15^{1+}$ and $y16^{1+}$ MS/MS fragment ions for both control and JLZ184-treated MAGL preparations (Figure 1C). The remaining serine, which is located in the portion of the active site peptide modified by JZL184, corresponds to the predicted catalytic nucleophile Ser122, based on previous studies (Karlsson et al., 1997) and the complete conservation of this residue across all MAGL orthologs and distantly homologous serine hydrolases. We therefore recombinantly expressed and purified a MAGL mutant in which the catalytic Ser122 was mutated to an alanine (MAGL-S122A). Upon incubation with JZL184, digestion with trypsin, and LC-MS/MS analysis, we detected a peak with $m/z$ = 1308.96 corresponding to the 4+ charge state of the unmodified MAGL-S122A active site tryptic peptide, but did not detect a peak corresponding to the JZL184-adduct of this peptide (Figure S2). Collectively, these data indicate that JZL184 inactivates MAGL by covalent carbamoylation of the enzyme's catalytic nucleophile Ser122.

To assess the stability of the JZL184-MAGL adduct, we measured the rate of decarbamoylation of this complex by incubating recombinant MAGL overexpressed in COS7 cells with JZL184 and then using size-exclusion chromatography to remove unreacted JZL184. MAGL activity was then measured by 2-AG hydrolysis assays over a period of 30 hr at room temperature. Less than 10% recovery of enzyme activity was observed over this period (Figure 1D), indicating that the JZL184-MAGL adduct is very stable.

## An Optimized Vehicle Delivery System for In Vivo Analysis of JZL184

In our initial disclosure of JZL184, we administered the compound intraperitoneally (i.p.) to mice in a polyethylene glycol (PEG) vehicle (Long et al., 2009) because this vehicle best solubilized JZL184 (Figure S3). However, we have found that the PEG vehicle can confound certain metabolomic measurements, especially in peripheral tissues where PEG can accumulate and reside for extended periods. Owing to the popularity of saline-emulphor vehicles for delivering inhibitors and other pharmacological agents (Fegley et al., 2005; Lichtman et al., 2001; Verty et al., 2003), we explored the possibility of administering JZL184 in an 18:1:1 solution of saline:emulphor:ethanol. Simple addition of JZL184 to this vehicle resulted in poor solubility and in vivo activity (as judged by lack of MAGL inhibition in brain tissue; data not shown). However, extensive sonication of JZL184 in the saline-emulphor vehicle produced a uniform suspension (Figure S3) that could be administered to rodents by intraperitoneal injection to efficiently inactivate MAGL in vivo.

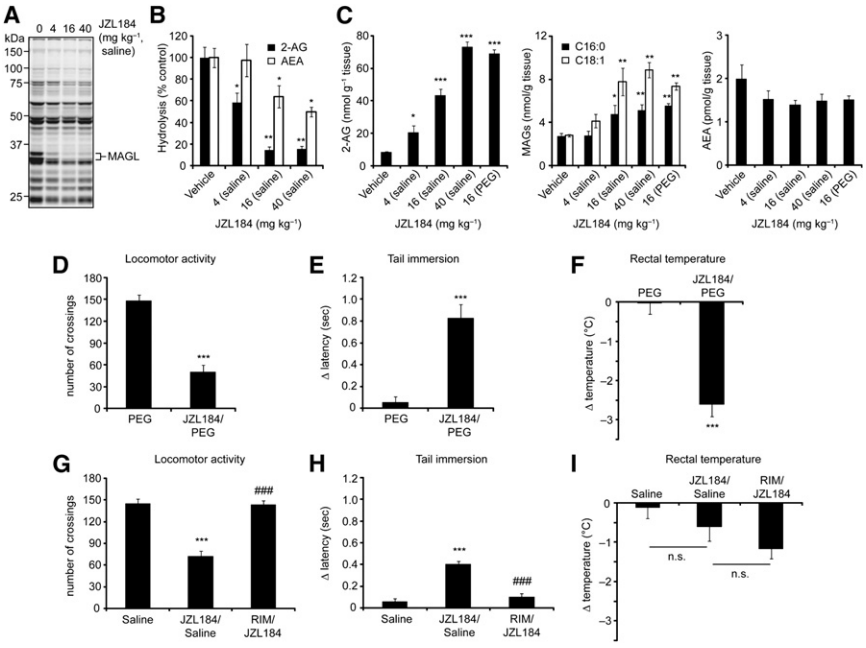


**Figure 2. Comparison of Vehicles for JZL184 Administration to Mice**

(A, B) Serine hydrolase activity profiles as determined by reactivity with the ABPP probe FP-rhodamine (A, fluorescent gel shown in grayscale) and 2-AG and AEA hydrolysis activity assays (B) of brain membranes prepared from mice treated with JZL184 (saline-emulphor, i.p., 4–40 mg $kg^{-1}$, 4 hr).

(C) Total brain 2-AG, PG (C16:0), OG (C18:1), and AEA measurements from mice treated with JZL184 (4–40 mg $kg^{-1}$) in the indicated vehicle for 4 hr.

(D–I). Locomotor activity (D, G), thermal pain sensation (E, H), and rectal temperature (F, I) of mice treated with JZL184 in the PEG (16 mg $kg^{-1}$, i.p., 4 hr; *upper panels*) or saline-emulphor (40 mg $kg^{-1}$, i.p., 4 hr; *lower panels*) vehicle. Mice in either treatment group were not cataleptic. Administration of the CB1 antagonist rimonabant (RIM, i.p., 3 mg $kg^{-1}$) to mice 15 min before JZL184 treatment blocked the observed behavioral effects in the saline-emulphor group (D–F, lower panels). RIM has previously been shown to block the behavioral effects of JZL184 administered in the PEG vehicle (Long et al., 2009). *p < 0.05, **p < 0.01, ***p < 0.001 for inhibitor-treated versus vehicle-treated animals; ### p < 0.001 for RIM- and inhibitor-treated versus inhibitor-treated animals.

Data are presented as mean ± SEM. For B and C, n = 3–6/group; for D–F, n = 10–18/group.

We directly compared the PEG and saline-emulphor delivery systems for JZL184 by measuring brain MAGL activity and lipid levels from inhibitor-treated mice. C57Bl/6 mice were treated with JZL184 (4–40 mg $kg^{-1}$, 18:1:1 saline:ethanol:emulphor vehicle, i.p. or 16 mg $kg^{-1}$, PEG vehicle, i.p.) and killed after 4 hr for analysis. JZL184 in both vehicles produced near-complete and selective blockade of MAGL activity as judged by competitive ABPP with the serine hydrolase-directed probe fluorophosphonate (FP)-rhodamine (Patricelli et al., 2001) (Figure 2A) or 2-AG hydrolytic substrate assays (Figure 2B), which was accompanied by dramatic elevations in 2-AG (Figure 2C, *left panel*) and more modest changes in other MAGs such as mono-palmitoylglycerol (C16:0 MAG) and mono-oleoylglycerol (C18:1 MAG) (Figure 2C, *middle panel*). A slightly higher dose of JZL184 was required in the saline-emulphor vehicle to achieve the same 2-AG elevations as observed with the PEG vehicle (40 mg $kg^{-1}$ versus 16 mg $kg^{-1}$, respectively; Figure 2C, *left panel*). JZL184 showed excellent selectivity in the nervous system, because this agent did not block FP-rhodamine labeling of other brain hydrolases (Figure 2A) and showed only modest inhibition of FAAH activity (~50% at the highest dose tested, Figure 2B) that did not produce changes in brain AEA levels (Figure 2C, *right panel*). These observations are consistent with previous reports that >85% FAAH inhibition is required to observe bulk (Ahn et al., 2009; Fegley et al., 2005) or stimulated (Long et al., 2009) changes in AEA levels in the nervous system. 2-AG was similarly elevated in FAAH (−/−) mice (Cravatt et al., 2001) treated with JZL184 (Figure S4), demonstrating that genetic disruption of FAAH does not alter brain 2-AG metabolism by MAGL.

Consistent with our previous report (Long et al., 2009), JZL184 administered in a PEG vehicle was found to cause three of the four behavioral effects of the tetrad test characteristic of direct CB1 agonists, namely, hypomotility (Figure 2D), analgesia (Figure 2E), and hypothermia (Figure 2F), but not catalepsy. Interestingly, a slightly different profile was observed for JZL184 in the saline-emulphor vehicle (40 mg $kg^{-1}$, i.p., 4 hr), where we observed significant CB1-dependent hypomotility (Figure 2G) and analgesia (Figure 2H), but not hypothermia (Figure 2I). The discrepancy in the hypothermic effects of JZL184 administered in different vehicles might be explained in part by the fact that the PEG vehicle alone (but not the saline-emulphor vehicle) caused a transient drop in body temperature, which might suggest that blockade of MAGL causes dysregulation of temperature homeostasis following a hypothermic insult.

## Evaluating the Inhibition of MAGL in Liver by JZL184

We next set out to assess the ability of JZL184 to inhibit MAGL outside of the nervous system. C57Bl/6 mice were treated with JZL184 (16 mg $kg^{-1}$ in saline-emulphor, i.p.), killed 15 min, 45 min, 2 hr, or 4 hr after treatment, and liver tissues removed for analysis. MAGL inactivation in liver, as judged by 2-AG hydrolysis or competitive ABPP assays, was extremely rapid, reaching near completion by the first time point analyzed (15 min, Figure 3A). We observed a residual 20% 2-AG hydrolytic activity that was insensitive to JZL184 (Figure 3B), indicating that, like in brain (Blankman et al., 2007; Long et al., 2009), additional enzymes in liver might catalyze this reaction. In contrast to the rapid inactivation of MAGL by JZL184, FAAH was inhibited much more slowly, with ~50% FAAH activity still observed at 4 hr after treatment (Figure 3B). Lipid profiles revealed significant elevations in 2-AG and C16:0 and C18:1 MAGs in liver tissue from JZL184-treated mice that peaked between 2 and 4 hr after inhibitor treatment.

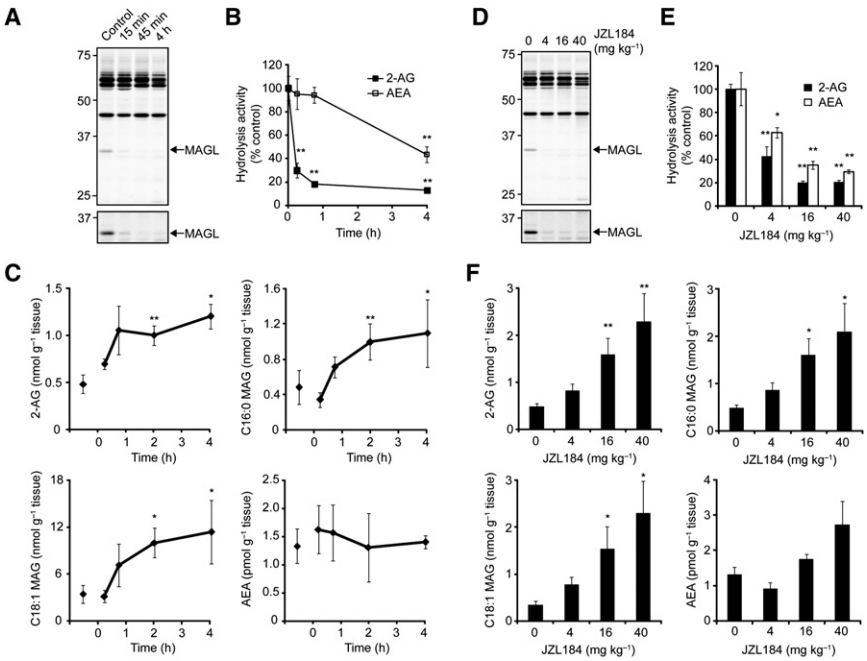


**Figure 3. Time Course and Dose-Response Analysis of MAGL Inactivation by JZL184 in Liver**

(A and B) Serine hydrolase activity profiles as judged by FP-rhodamine labeling (A) and 2-AG and AEA hydrolysis assays (B) of liver membranes from mice treated with JZL184 (16 mg $kg^{-1}$ in saline-emulphor, i.p.) for the indicated times.

(C) Liver 2-AG (C20:4), PG (C16:0), OG (C18:1), and AEA levels from mice treated with JZL184 (16 mg $kg^{-1}$ in saline-emulphor, i.p.) for the indicated times.

(D and E) Serine hydrolase activity profiles (D) and 2-AG and AEA hydrolysis assays (E) of liver membranes from mice treated with JZL184 at the indicated doses (4–40 mg $kg^{-1}$, i.p., 4 hr).

(F) Liver 2-AG (C20:4), PG (C16:0), OG (C18:1), and AEA levels from mice treated with JZL184 at the indicated doses (4–40 mg $kg^{-1}$ in saline-emulphor, i.p., 4 hr). *$p < 0.05$, **$p < 0.01$ for inhibitor-treated versus vehicle-treated animals. Data are presented as mean ± SEM; n = 3–4/group.

(A and D) Lower gels show higher intensity of imagoes of the MAGL signals.

No changes in AEA levels were detected in liver at any time point after JZL184 treatment (Figure 3C). C57Bl/6 mice treated with increasing amounts of JZL184 (4–40 mg $kg^{-1}$, i.p., saline-emulphor, 4 hr) showed dose-dependent decreases in MAGL activity by competitive ABPP (Figure 3D) and substrate hydrolysis assays (Figure 3E) that correlated with dose-dependent elevations in liver MAGs (Figure 3F). No change in liver AEA was observed at any of the doses tested ($p > 0.20$) (Figure 3F).

Competitive ABPP experiments revealed that JZL184 maintained excellent selectivity for MAGL in liver tissue, especially at early time points (<45 min, 16 mg $kg^{-1}$) (Figure 3A). At longer time points (4 hr; Figure 3A) or higher doses (40 mg $kg^{-1}$; Figure 3D), we observed a partial decrease in probe labeling signals for multiple proteins in the 50–65 kDa region, which likely correspond to carboxylesterases that are known to be sensitive to a variety of carbamate-based inhibitors (Ahn et al., 2007; Alexander and Cravatt, 2005; Zhang et al., 2007).

## A Comprehensive Profile of MAGL Inactivation in Peripheral Tissues

The heightened magnitude of accumulation of 2-AG in brain versus liver tissue from JZL184-treated animals suggested that the former tissue exhibits greater capacity to produce this endocannabinoid. To better understand the relative level of endocannabinoid tone across different tissues, we evaluated MAGL activity and lipid profiles in brain, liver, kidney, spleen, heart, testis, lung, and white (WAT) and brown (BAT) adipose tissue from vehicle- and JZL184-treated mice. C57Bl/6 mice were treated with JZL184 at 16 mg $kg^{-1}$ in saline-emulphor, killed at 2 hr, and their tissues were harvested. We detected a 33 kDa, JZL184-sensitive band by gel-based ABPP in every tissue proteome analyzed (Figures 4A–4I). In brain and testis, a 35 kDa form of MAGL was also observed by gel-based ABPP, as reported previously (Blankman et al., 2007; Long et al., 2009), perhaps reflecting an additional splice isoform of MAGL in these tissues (Karlsson et al., 2001). Despite producing an equivalent and near-complete blockade of MAGL activity in each tissue (as judged by FP-rhodamine labeling), JZL184 inhibited 2-AG hydrolysis activity in these tissues to varying extents. For most tissues, a >50% block of 2-AG hydrolysis activity was observed in JZL184-treated animals (Figure 4). BAT and WAT, however, showed only modest 30% decreases in activity (Figures 4F and 4G), possibly reflecting the action of other 2-AG hydrolases in these fat tissues, such as hormone-sensitive lipase, that are insensitive to JZL184.

Individual tissues showed markedly different extents and patterns of MAG accumulation following MAGL inhibition by JZL184. As reported previously, brain exhibited a dramatic (>5-fold) increase in 2-AG levels, but more modest (~2-fold) increases in C16:0 and C18:1 MAGs. Liver, kidney, spleen, heart, and BAT showed significant ($p < 0.05$) elevations across the entire panel of MAG species analyzed, with the largest elevations being observed in the C16:0 and C18:1 species (Figures 4B–4F). WAT and lung, however, did not show elevations in 2-AG, but accumulated both C16:0 and C18:1 MAG (Figures 4G and 4H). Finally, despite the presence of MAGL in testis and its inactivation by JZL184 as judged by ABPP and 2-AG hydrolysis assays, we did not observe any significant changes ($p > 0.05$) in any MAG species in this tissue (Figure 4I). We also did not observe any significant accumulation ($p > 0.05$) of AEA in any of the tissues in this analysis (Figures 4A–4I). Lastly, we confirmed that JZL184 reduced arachidonic acid levels in brain (Table S1) as had been previously reported (Long et al., 2009; Nomura et al., 2008b), but found no changes in palmitic, stearic, oleic, or arachidonic acid levels in any of the peripheral tissues analyzed (Figure S5).

## Selectivity Profiling of JZL184 in Peripheral Mouse Tissues

The pharmacological value of JZL184 for characterizing the physiological functions of MAGL depends on the selectivity of this

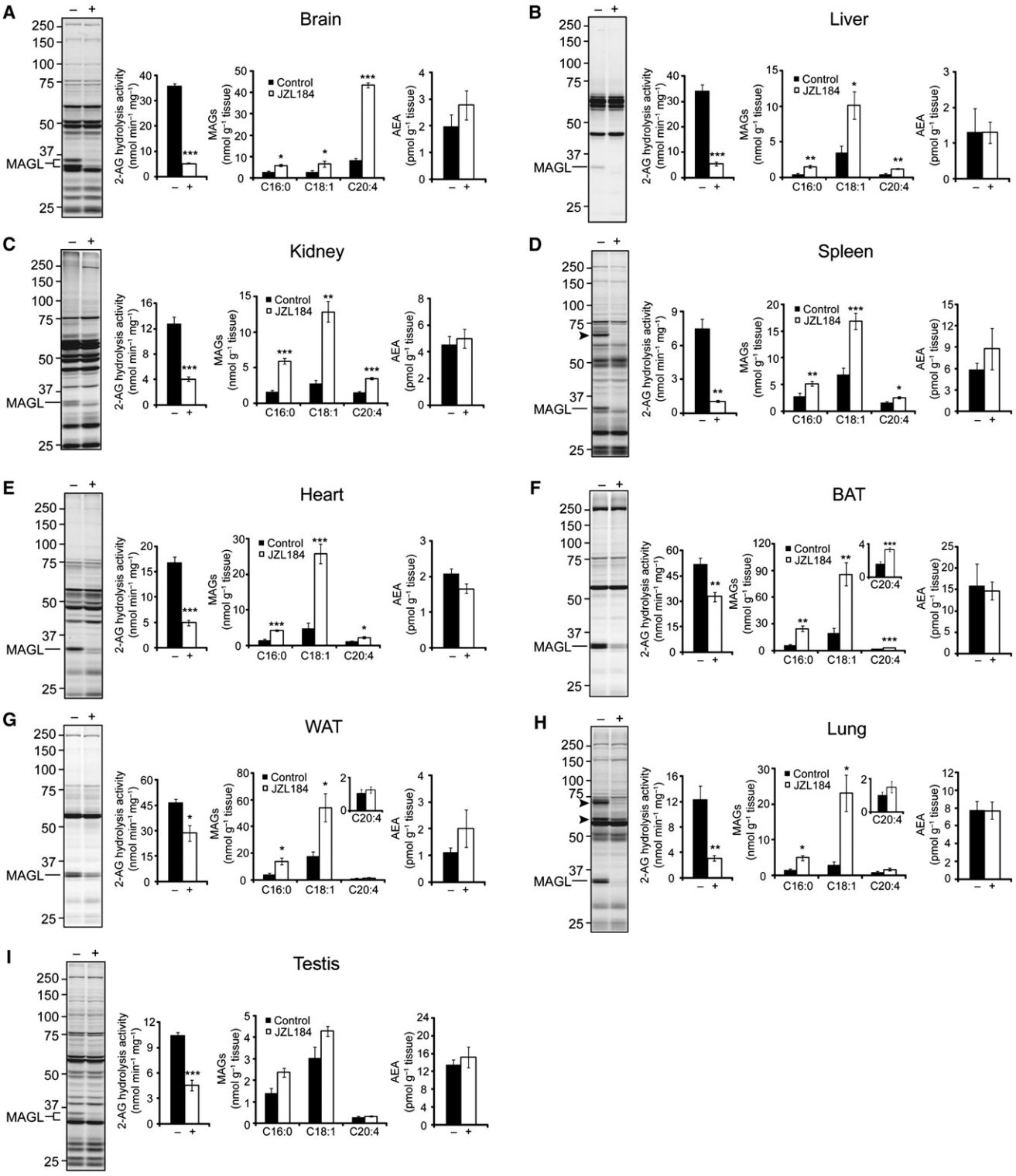


**Figure 4. A Comprehensive Biochemical Profile of MAGL Inactivation in Tissues for JZL184-Treated Mice**

(A–I) Serine hydrolase activity profiles as judged by FP-rhodamine labeling, 2-AG hydrolysis activity, and levels of MAGs and AEA in brain (A), liver (B), kidney (C), spleen (D), heart (E), brown adipose tissue (BAT) (F), white adipose tissue (WAT) (G), lung (H), and testis (I) from mice treated with JZL184 (16 mg $kg^{-1}$ in saline-emulphor, i.p., 2 hr). JZL184 off-targets are indicated by arrowheads. The 2 hr metabolic data from liver is from the time course analysis presented in Figure 3C. *$p < 0.05$, **$p < 0.01$, ***$p < 0.001$ for inhibitor-treated versus vehicle-treated animals. Data are presented as mean ± SEM; n = 4–6/group.

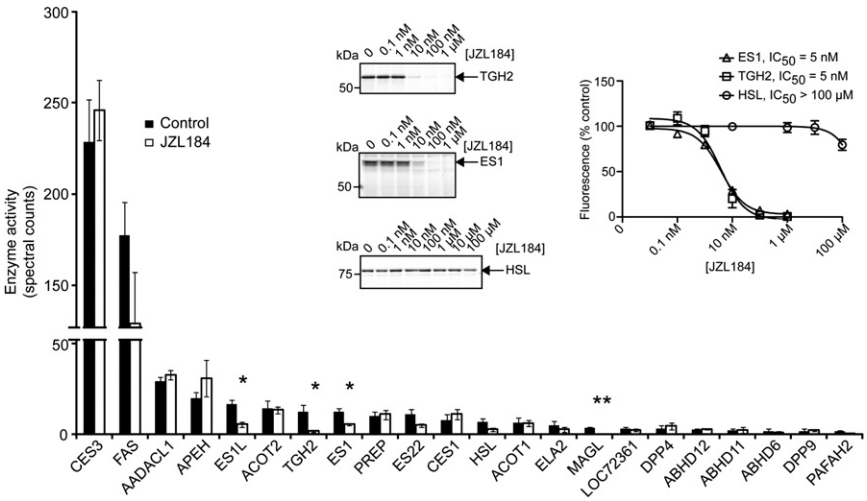


**Figure 5. ABPP-MudPIT Analysis of Lung Membrane Proteomes from Mice Treated with JZL184 (16 mg kg$^{-1}$, i.p., 2 hr)**

(Insert) Competitive ABPP measuring JZL184 blockade of FP-rhodamine for ES1, TGH2, and HSL recombinantly expressed in COS7 cells (left insert, representative competitive ABPP gels; right insert, quantification of blockade of FP-rhodamine labeling). Data are presented as mean ± SEM of three independent experiments. *p < 0.05, **p < 0.01, for inhibitor-treated versus vehicle-treated animals.

inhibitor. Of the nine tissues analyzed by competitive ABPP from JZL184-treated mice, only spleen and lung contained detectable off-target(s), which migrated between 60 and 75 kDa. To further characterize these peripheral off-targets of JZL184, we analyzed lung membrane proteomes using an advanced LC-MS platform, termed ABPP-MudPIT, that displays enhanced resolution and sensitivity compared with gel-based ABPP (Jessani et al., 2005). Briefly, lung membrane proteomes from mice treated with JZL184 or vehicle were subjected to competitive ABPP with the biotinylated fluorophosphonate (FP) probe, FP-biotin (Liu et al., 1999). FP-biotin-labeled proteins were then enriched with avidin, digested on-bead with trypsin, analyzed by multidimensional LC-MS, and identified and quantified using the SEQUEST search algorithm (Eng et al., 1994) and spectral counting (Liu et al., 2004), respectively. ABPP-MudPIT confirmed that JZL184 (16 mg kg$^{-1}$ in saline-emulphor, i.p., 2 hr) completely inhibited MAGL in lung membrane proteomes and also identified three additional targets of this compound, all from the carboxylesterase family: esterase 1 (ES1), esterase 1-like (ES1L), and carboxylesterase ML1 (also annotated as a second triglyceride hydrolase, TGH2 [Okazaki et al., 2006]) (Figure 5 and Table S2). The spectral count signals for hormone-sensitive lipase (HSL) were also lower in JZL184-treated lung proteomes, although this reduction did not reach statistical significance. To confirm whether these enzymes were valid targets of JZL184, we recombinantly expressed ES1, TGH2, and HSL in COS7 cells and evaluated them for sensitivity to JZL184 by competitive ABPP. JZL184 inhibited FP-rhodamine labeling of both ES1 and TGH2 (Figure 5) with potencies comparable to the inhibition of recombinant mouse MAGL (Long et al., 2009; Nomura et al., 2008b). In contrast, FP-rhodamine labeling of recombinant HSL was not impaired (Figure 5), confirming that this hydrolase is not a target of JZL184. Collectively, these functional proteomic data indicate that JZL184 maintains excellent selectivity for MAGL across most mouse tissues, targeting only a limited number of additional hydrolases in a subset of peripheral tissues.

### JZL184 Is Equipotent against Human and Mouse MAGL, but Less Active against Rat MAGL

To understand the scope of JZL184 activity against different MAGL orthologs, we recombinantly expressed mouse, rat, and human MAGL in COS7 cells and measured JZL184 inactivation of these enzymes in vitro by substrate assays (Figure 6A). JZL184 inhibited mouse and human MAGL with equal potency, but showed ~10-fold lower activity against rat MAGL (Figure 6B). We confirmed the lower potency of JZL184 against rat MAGL by in vitro competitive ABPP analysis of mouse and rat brain membranes (Figures 6C and 6D). JZL184 also appears to show a similar reduction in activity against rat FAAH, resulting in an overall similar relative selectivity windows for MAGL over FAAH in both mouse and rat brain proteomes (Figure 6D). Lastly, JZL184 showed equivalent potency against rat and mouse ABHD6 (Figure 6D), a second 2-AG hydrolase expressed in brain (Blankman et al., 2007).

## DISCUSSION

Despite its molecular characterization over a decade ago (Karlsson et al., 1997), the physiological functions of MAGL have remained relatively enigmatic due to a dearth of pharmacological tools or genetic models to test the enzyme's function in vivo. We recently introduced an efficacious and selective inhibitor of MAGL, termed JZL184, and showed that this agent can selectively block MAGL activity in the nervous system of mice (Long et al., 2009; Nomura et al., 2008b). However, the mechanism by which JZL184 inhibits MAGL, as well as the scope of its inhibitory effect on MAGL in various tissues, remained unknown. Here, we provide clear evidence that JZL184 acts as a long-lasting irreversible inhibitor of MAGL by carbamoylating the enzyme's serine nucleophile. We furthermore show that JZL184 inactivates MAGL with good efficacy and selectivity in a wide range of central and peripheral tissues.

Interestingly, the impact of MAGL blockade on endocannabinoid/MAG metabolism differed markedly in individual tissues. In brain, both the basal level of 2-AG (5–10 nmol/g) and its fold-elevation following MAGL inhibition (>5-fold) were much higher than in any peripheral tissue (Figure 4A). In contrast, several peripheral tissues from JZL184-treated mice accumulated substantial quantities of C16:0 and C18:1 MAGs (the two species that were only modestly elevated in brain), while showing little or no elevation in 2-AG (Figure 4). These data, in addition to the high relative expression of CB1 in the brain compared with peripheral tissues (Mackie, 2005), might suggest enhanced tonic levels of 2-AG metabolism and signaling in the nervous system compared

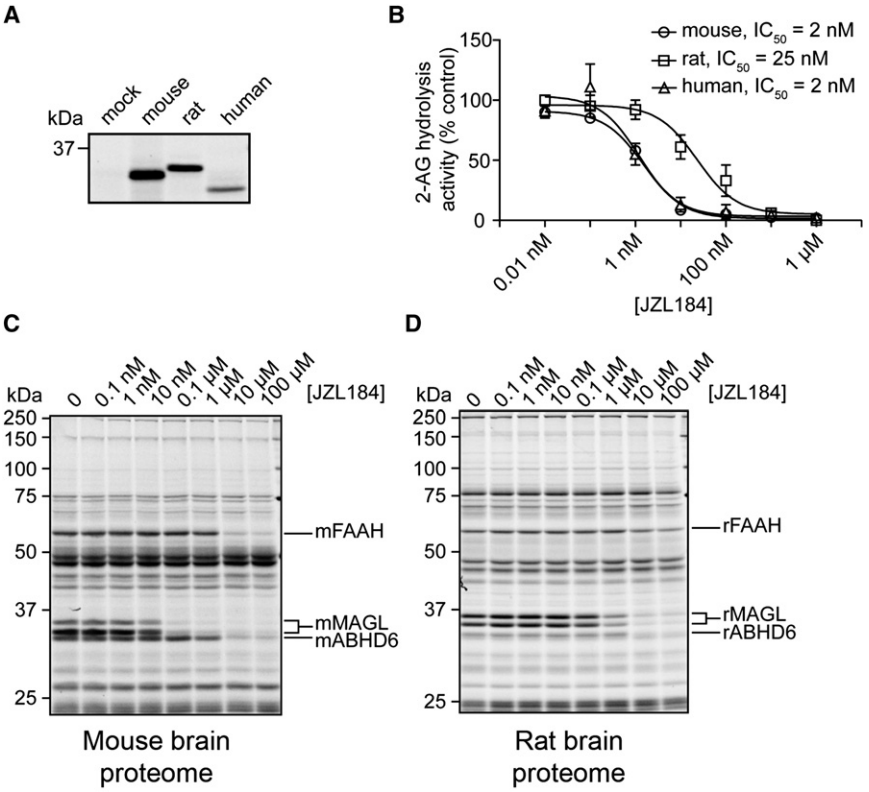


**Figure 6. Characterization of JZL184 Inhibition of Mouse, Rat, and Human MAGL**

(A) FP-rhodamine labeling of recombinant mouse, rat, and human MAGL expressed in COS7 cells (1 μM FP-rhodamine, 30 min).

(B) Blockade of recombinant MAGL orthologs by JZL184 as determined by substrate assays with 2-AG. Data are presented as mean ± SEM of three independent experiments.

(C and D) Competitive ABPP showing the effect of JZL184 on serine hydrolase activities in the mouse (C) and rat (D) brain membrane proteomes.

For B–D, JZL184 was incubated with cell/tissue lysates (30 min, 37°C) at the indicated concentrations, followed by addition of 2-AG (100 μM, 5 min, room temperature) (B) or FP-rhodamine (1 μM, 30 min, room temperature) (C and D). For C and D, control proteomes were treated with DMSO alone. Note that mouse and rat brain MAGL migrates as a 33 and 35 kDa doublet by SDS-PAGE, as reported previously (Blankman et al., 2007; Long et al., 2009).

with peripheral tissues. Conversely, the more dramatic elevations in C16:0 and C18:1 MAGs observed in some peripheral tissues following MAGL blockade might reflect a more general metabolic function for this enzyme at these sites. Another feature distinctive to MAGL in the nervous system is its regulation of brain arachidonic acid levels (Table S1), which was not observed in any peripheral tissues (Figure S5). These data again underscore differences in the function of MAGL in the brain and the periphery.

Because all tissues analyzed from JZL184-treated mice showed >90% inhibition of MAGL as judged by gel-based ABPP (Figure 4), we presume that the distinct MAG profiles observed in individual tissues upon JZL184 treatment arise from other factors such as the presence of additional MAG hydrolases or different capacities for MAG biosynthesis. The former possibility seems likely in organs, such as WAT, where other enzymes that display MAG hydrolytic activity, such as HSL, are present at high levels (Fredrikson and Belfrage, 1983; Osuga et al., 2000). The latter possibility is supported by preliminary time-course experiments, which have revealed similar relative rates of 2-AG accumulation in the brain and liver upon JZL184 treatment, but distinct plateau values for elevations in this endocannabinoid (11- and 4-fold, respectively) (Figure S5). Regardless of the precise mechanism, tissue-specific differences in endocannabinoid metabolism might help to explain the diversity of physiological functions performed by this lipid signaling system. Indeed, recent evidence suggests that CB1 antagonists affect metabolism, at least in part, by disrupting endocannabinoid pathways at peripheral sites such as liver (Osei-Hyiaman et al., 2008) and adipocytes (Motaghedi and McGraw, 2008). Determining how the local concentrations of endocannabinoids are regulated at these peripheral sites is critical to achieve a full understanding of the mechanism of action of these signaling lipids.

Our studies also point to two areas for future improvement of MAGL inhibitors. First, although competitive ABPP confirmed that JZL184 generally displays high selectivity for MAGL, a handful of additional targets were discovered in select peripheral tissues. That these "off-targets" corresponded to carboxylesterases is not surprising, given that other carbamates, such as the FAAH inhibitor URB597, have also been shown to inhibit carboxylesterases (Alexander and Cravatt, 2005; Zhang et al., 2007). Although we have previously demonstrated that JZL184 does not interact with other components of the endocannabinoid system (Long et al., 2009), we cannot exclude the possibility that JZL184 interacts with other proteins outside of the serine hydrolase superfamily, such as cytochrome P450 enzymes, that might also participate in lipid metabolism (Chen et al., 2008). Although the inhibition of carboxylesterases and other potential off-targets could complicate interpretation of JZL184's pharmacological effects in certain peripheral tissues, assessing the reversibility of observed effects by cannabinoid receptor antagonists should clarify whether they are due to the enhanced 2-AG signaling or a different mechanism. Regardless, having defined the principal off-targets of JZL184 through functional proteomic profiling, we are in good position to move forward with directed medicinal chemistry efforts to improve the selectivity of this inhibitor. A second feature of JZL184 to consider for future refinement is species selectivity. JZL184 potently inhibited both mouse and human MAGL, but showed a 10-fold reduced activity against rat MAGL. Because rats are extensively used as a model system for studying higher-order behaviors, it would be beneficial to develop inhibitors with improved activity against rat MAGL. However, this task might prove difficult to accomplish using the piperidine carbamate scaffold of JZL184, because our

preliminary work with other inhibitors from this class has revealed a consistent trend toward higher potency for mouse and human MAGL over rat MAGL (our unpublished observations). Considering the high sequence identity shared by the three MAGL orthologs (92% between mouse and rat MAGL and 84% between mouse and human MAGL), we anticipate that structural studies might be required to clarify their surprising differences in sensitivity to JZL184 and related compounds.

## SIGNIFICANCE

**Monoacylglycerol lipase (MAGL) is a principal degradative enzyme for the endocannabinoid 2-arachidonoylglycerol (2-AG). Selective inhibitors of MAGL are therefore of value as both research tools to study the physiological functions of the endocannabinoid system and potential pharmaceutical agents to perturb this system for therapeutic gain. Here, we have shown that the piperidine carbamate JZL184 irreversibly inactivates MAGL by carbamoylation of the enzyme's catalytic serine nucleophile. This inhibition is observed in vivo with high selectivity in both central and peripheral tissues, enabling a comprehensive analysis of the contribution that MAGL makes to the metabolism of 2-AG and other monoglycerides. Interestingly, our studies provide evidence for marked tissue-specific differences in endocannabinoid tone, with brain showing the most dramatic elevations in 2-AG following MAGL blockade. In contrast, MAGL's control over the levels of 2-AG and other monoglycerides varied considerably in peripheral tissues, even in cases where this enzyme was largely responsible for bulk 2-AG hydrolytic activity. These data thus point to organs where MAGL-regulated 2-AG signaling might have its most profound effects on physiology and, conversely, to tissues where other enzymes might contribute to 2-AG and monoglyceride metabolism in vivo.**

## EXPERIMENTAL PROCEDURES

### Materials

2-AG, $d_5$-2-AG, AEA, $d_4$-AEA, $d_4$-PEA, and pentadecanoic acid were purchased from Cayman Chemicals. Monopentadecanoin and monoheptadecanoin were purchased from Nu-Chek-Prep, Inc. FP-rhodamine (Patricelli et al., 2001), FP-biotin (Liu et al., 1999), and JZL184 (Long et al., 2009) were synthesized as described previously.

### Expression and Purification of Recombinant MAGL and MAGL-S122A

Human MAGL was polymerase chain reaction (PCR) amplified using the following primers: forward, GACTGGATCCCATGCCAGAGGAAAGTTC; reverse, CAGTAAGCTTTCAGGGTGGGGACGCAGTTC. The PCR product was subsequently cloned into pET-45b(+) (Novagen) using BamHI and HindIII restriction sites. The resulting hMAGL-pET45b(+) construct was transformed into BL21(DE3) cells (Invitrogen) for expression. A single colony from a fresh transformation was used to inoculate an overnight culture in a media of LB containing 100 μg ml$^{-1}$ carbenicillin (LB$^{carb}$), incubated at 37°C with shaking (225 rpm). The following morning, the overnight culture was used to seed the induction culture at a ratio of 1:100. The induction culture was incubated at 37°C with shaking (225 rpm) and the $OD_{600}$ was monitored each hour. Once the $OD_{600}$ reached 0.4–0.6 1 mM IPTG was added each induction culture and allowed to incubate for additional 4 hr. Cells were harvested by centrifugation at 6000 x *g* for 10 min at 4°C. Cell pellets were stored at −80°C. To purify 6xHIS-hMAGL, cell pellets from a 1 l culture were thawed at room temperature in a buffer containing 50 mM Tris (pH 8.0), 200 mM NaCl, 1% LDAO, lysozyme (0.25 mg ml$^{-1}$), and DNase I (25 μg ml$^{-1}$) with constant stirring for ~10 min, after which cells were lysed by sonication. The soluble and insoluble materials were separated by centrifugation at 24,000 x g for 30 min at 4°C. The resulting supernatant was batch loaded with 0.5 ml TALON Metal Affinity Resin (Clontech) (50% slurry) for 1 hr at 4°C. The loaded resin was added to a column and washed with 10 column volumes (CV) of 50 mM Tris (pH 8.0), 200 mM NaCl (wash buffer), 10 CV wash buffer containing 5 mM imidazole, 10 CV of wash buffer containing 10 mM imidazole, and eluted with wash buffer containing with 200 mM imidazole. The eluted protein was subsequently concentrated using an Amicon Ultra centrifugal filter device (Millipore) with 10,000 molecular weight cut-off and the protein concentration determined using $D_C$ Protein Assay (Bio-Rad). A typical 1 l pellet (~1.5 g) will yield ~1.5 mg MAGL of single band purity when analyzed by SDS-PAGE and stained with Coomassie blue.

The MAGL-S122A construct was created using the following primers: sense, CTTCTGGGCCACGCCATGGGAGGCG; antisense, CGCCTCCCATGGCGTGGCCCAGAAG, and the Stratagene QuikChange II Site-Directed Mutagenesis kit according to the manufacturer's protocols.

### LC-MS/MS Detection of Modified and Unmodified Tryptic Peptides from JZL184-Treated Preparations of MAGL

Purified, recombinant hMAGL (50 μl, 5 mg ml$^{-1}$) was incubated with DMSO (1 μl) or JZL184 (1 μl, 200 μM final) for 20 min at room temperature. Urea (100 mg) was added to each reaction and the reactions were diluted with phosphate-buffered saline (PBS, 150 μl). Each sample was then subsequently incubated with *tris*-(2-carboxyethyl)phosphine (TCEP, 5 mM) and iodoacetamide (10 mM) for 30 min each at room temperature. The samples were diluted again with ammonium bicarbonate (25 mM, 550 μl) and subjected to trypsin digestion overnight at 37°C. The next day, samples were concentrated, resuspended in ammonium bicarbonate (25 mM, 200 μl) with 0.1% formic acid, and a 10 μl aliquot was pressure loaded onto a 100 μm (inner diameter) fused silica capillary column with a 5 μm tip that contained 10 cm C18 resin (aqua 5 μm, Phenomenex). LC-MS/MS analysis was performed on an LTQ-Orbitrap mass spectrometer (ThermoFisher) coupled to an Agilent 1100 series HPLC. Peptides were eluted from the column using a 125 min gradient of 5%–100% Buffer B (Buffer B: 20% water, 80% acetonitrile, 0.1% formic acid). The flow rate through the column was 0.25 μl min$^{-1}$ and the spray voltage was 2.5 kV. The LTQ was operated in data-dependent scanning mode, with one full MS scan (400–1600 *m/z*) followed by seven MS/MS scans of the $n^{th}$ most abundant ions with dynamic exclusion enabled.

### Measurement of Reversibility of JZL184-MAGL Reaction

Recombinant mMAGL overexpressed in COS7 cells was diluted in Tris buffer (50 mM [pH 8], 1 mg ml$^{-1}$ final concentration, 130 μl final volume) and incubated with JZL184 (100 μM) or DMSO for 30 min at room temperature. The samples were then subjected to a PD10 size exclusion column (GE Healthcare), concentrated to 200 μl, and incubated at room temperature. At the indicated times, an aliquot of each sample was removed and substrate hydrolysis activity was determined exactly as described below.

### Preparations of Mouse and Rat Tissue Proteomes

Tissues were Dounce-homogenized in PBS (pH 7.5), followed by a low-speed spin (1400 x *g*, 5 min) to remove debris. The supernatant was then subjected to centrifugation (64,000 x *g*, 45 min) to provide the cytosolic fraction in the supernatant and the membrane fraction as a pellet. The pellet was washed and resuspended in PBS buffer by sonication. Total protein concentration in each fraction was determined using a protein assay kit (Bio-Rad). Samples were stored at −80°C until use.

### Competitive ABPP Experiments

Tissue proteomes were diluted to 1 mg ml$^{-1}$ in PBS and FP-rhodamine was added at a final concentration of 1 μM in a 50 μl total reaction volume. After 30 min at 25°C, the reactions were quenched with 4x SDS-PAGE loading buffer, boiled for 5 min at 90°C, subjected to SDS-PAGE, and visualized in-gel using a flatbed fluorescence scanner (Hitachi). For experiments involving a preincubation with inhibitor, the reactions were prepared without FP-rhodamine. JZL184 was added at the indicated concentration and incubated for 30 min at 37°C. FP-rhodamine was then added and the reaction was carried out exactly

as described above. For ABPP-MudPIT studies, a portion of the lung membrane proteome (0.5 ml, 1 mg $ml^{-1}$ in PBS) from the mice treated with JZL184 or vehicle as described above was labeled with 5 μM FP-biotin for 2 hr at room temperature and prepared for ABPP-MudPIT analysis as described previously (Jessani et al., 2005; Long et al., 2009), except that the Lys-C digestion step was omitted. MudPIT analysis of eluted peptides was carried out as previously described on a coupled Agilent 1100 LC-ThermoFinnigan LTQ-MS instrument. All data sets were searched against the mouse IPI database using the SEQUEST search algorithm (Eng et al., 1994) and the results were filtered and grouped with DTASELECT (Tabb et al., 2002). Peptides with cross-correlation scores greater than 1.8 (+1), 2.5 (+2), 3.5 (+3) and delta CN scores greater than 0.08 were included in the spectral counting analysis. Spectral counts are reported as the average of three samples with the standard error of the mean (SEM).

### Recombinant Expression of Enzymes in COS7 Cells

Enzymes were recombinantly expressed in COS7 using a previously described procedure (Blankman et al., 2007) as detailed in Supplemental Data.

#### *Enzyme Activity Assays*

MAGL and FAAH substrate hydrolysis assays were performed using previously described LC-MS assays (Blankman et al., 2007) as detailed in Supplemental Data.

### In Vivo Studies with JZL184

JZL184 was prepared as a saline-emulphor emulsion by vortexing, sonicating, and gently heating neat compound directly into an 18:1:1 v/v/v solution of saline:ethanol:emulphor (4, 1.6, or 0.4 mg $ml^{-1}$ final concentration), or as a homogeneous PEG solution by vortexing, sonicating, and gently heating neat compound directly into PEG300 (Fluka) (4 mg $ml^{-1}$ final concentration). Male C57Bl/6J mice (<6 months old, 20–28 g) were i.p. administered JZL184 or an 18:1:1 v/v/v saline:emulphor:ethanol vehicle at a volume of 10 μl $g^{-1}$ weight (40, 16, or 4 mg $kg^{-1}$ by the dilutions above) or a PEG vehicle at a volume of 4 μl $g^{-1}$ weight (16 mg $kg^{-1}$ by the dilution above). All experiments were performed with the saline-emulphor vehicle unless otherwise indicated. After the indicated amount of time, mice were anesthetized with isoflurane and killed by decapitation. Brains were removed, hemisected along the midsagittal plane, and each half was then flash frozen in liquid $N_2$. Two separate portions (~100 mg) of the other indicated tissues were also harvested and flash frozen in liquid $N_2$. One portion of each tissue was analyzed by gel-based ABPP and the other portion was used for metabolite analysis. Animal experiments were conducted in accordance with the guidelines of the Institutional Animal Care and Use Committee of The Scripps Research Institute.

### Measurement of Brain Lipids

Brain lipid measurements were determined using a slight modification from a previously described procedure (Long et al., 2009) as detailed in Supplemental Data.

### Mouse Behavioral Experiments

Locomotor activity was assessed in a Plexiglas cage (18 × 10 × 8.5 in) that was marked by 7 cm × 7 cm grids on the bottom of the cage. The number of grids traversed by the hind limbs was counted for 5 min. Nociception was then assessed in the tail immersion assay, where each mouse was handheld and 1 cm of the tail was submerged into a 56°C water bath. The latency for the mouse to withdrawal its tail was scored. Rectal temperature was assessed by inserting a thermocouple probe 1.2 cm into the rectum and temperature was determined using a telethermometer. Preinjection tail immersion latency and rectal temperature were also measured as a baseline for each mouse.

## SUPPLEMENTAL DATA

Supplemental Data include six figures, two tables, and Supplemental Methods and can be found with this article online at http://www.cell.com/chemistry-biology/supplemental/S1074-5521(09)00176-8.

## ACKNOWLEDGMENTS

We thank Tianyang Ji for assistance with the transfection of MAGL cDNAs, Jason R. Thomas for purified human MAGL, and the Cravatt lab for helpful discussion and critical reading of the manuscript. This work was supported by the US National Institutes of Health (DA017259, DA009789), the Helen L. Dorris Institute Child and Adolescent Neuro-Psychiatric Disorder Institute, and the Skaggs Institute for Chemical Biology.

Received: April 4, 2009
Revised: May 13, 2009
Accepted: May 19, 2009
Published: July 30, 2009

## REFERENCES

Ahn, K., Johnson, D.S., Fitzgerald, L.R., Liimatta, M., Arendse, A., Stevenson, T., Lund, E.T., Nugent, R.A., Nomanbhoy, T.K., Alexander, J.P., et al. (2007). Novel mechanistic class of fatty acid amide hydrolase inhibitors with remarkable selectivity. Biochemistry *46*, 13019–13030.

Ahn, K., Johnson, D.S., Mileni, M., Beidler, D., Long, J.Z., McKinney, M.K., Weerapana, E., Sadagopan, N., Liimatta, M., Smith, S.E., et al. (2009). Discovery and characterization of a highly selective FAAH inhibitor that reduces inflammatory pain. Chem. Biol. *16*, 411–420.

Alexander, J.P., and Cravatt, B.F. (2005). Mechanism of carbamate inactivation of FAAH: implications for the design of covalent inhibitors and in vivo functional probes for enzymes. Chem. Biol. *12*, 1179–1187.

Bar-On, P., Millard, C.B., Harel, M., Dvir, H., Enz, A., Sussman, J.L., and Silman, I. (2002). Kinetic and structural studies on the interaction of cholinesterases with the anti-Alzheimer drug rivastigmine. Biochemistry *41*, 3555–3564.

Blankman, J.L., Simon, G.M., and Cravatt, B.F. (2007). A comprehensive profile of brain enzymes that hydrolyze the endocannabinoid 2-arachidonoylglycerol. Chem. Biol. *14*, 1347–1356.

Chen, J.K., Chen, J., Imig, J.D., Wei, S., Hachey, D.L., Guthi, J.S., Falck, J.R., Capdevila, J.H., and Harris, R.C. (2008). Identification of novel endogenous cytochrome p450 arachidonate metabolites with high affinity for cannabinoid receptors. J. Biol. Chem. *283*, 24514–24524.

Cravatt, B.F., Giang, D.K., Mayfield, S.P., Boger, D.L., Lerner, R.A., and Gilula, N.B. (1996). Molecular characterization of an enzyme that degrades neuromodulatory fatty-acid amides. Nature *384*, 83–87.

Cravatt, B.F., Demarest, K., Patricelli, M.P., Bracey, M.H., Giang, D.K., Martin, B.R., and Lichtman, A.H. (2001). Supersensitivity to anandamide and enhanced endogenous cannabinoid signaling in mice lacking fatty acid amide hydrolase. Proc. Natl. Acad. Sci. USA *98*, 9371–9376.

Devane, W.A., Hanus, L., Breuer, A., Pertwee, R.G., Stevenson, L.A., Griffin, G., Gibson, D., Mandelbaum, A., Etinger, A., and Mechoulam, R. (1992). Isolation and structure of a brain constituent that binds to the cannabinoid receptor. Science *258*, 1946–1949.

Di Marzo, V., Bisogno, T., and De Petrocellis, L. (2007). Endocannabinoids and related compounds: walking back and forth between plant natural products and animal physiology. Chem. Biol. *14*, 741–756.

Dinh, T.P., Carpenter, D., Leslie, F.M., Freund, T.F., Katona, I., Sensi, S.L., Kathuria, S., and Piomelli, D. (2002). Brain monoglyceride lipase participating in endocannabinoid inactivation. Proc. Natl. Acad. Sci. USA *99*, 10819–10824.

Dinh, T.P., Kathuria, S., and Piomelli, D. (2004). RNA interference suggests a primary role for monoacylglycerol lipase in the degradation of the endocannabinoid 2-arachidonoylglycerol. Mol. Pharmacol. *66*, 1260–1264.

Eng, J.K., McCormack, A.L., and Yates, J.R. (1994). An approach to correlate tandem mass spectral data of peptides with amino acid sequences in a protein database. J. Am. Soc. Mass Spectrom. *5*, 976–989.

Fegley, D., Gaetani, S., Duranti, A., Tontini, A., Mor, M., Tarzia, G., and Piomelli, D. (2005). Characterization of the fatty acid amide hydrolase inhibitor cyclohexyl carbamic acid 3′-carbamoyl-biphenyl-3-yl ester (URB597): effects

 

on anandamide and oleoylethanolamide deactivation. J. Pharmacol. Exp. Ther. *313*, 352–358.

Fredrikson, G., and Belfrage, P. (1983). Positional specificity of hormone-sensitive lipase from rat adipose tissue. J. Biol. Chem. *258*, 14253–14256.

Fredrikson, G., Tornqvist, H., and Belfrage, P. (1986). Hormone-sensitive lipase and monoacylglycerol lipase are both required for complete degradation of adipocyte triacylglycerol. Biochim. Biophys. Acta *876*, 288–293.

Jessani, N., Niessen, S., Wei, B.Q., Nicolau, M., Humphrey, M., Ji, Y., Han, W., Noh, D.Y., Yates, J.R., 3rd, Jeffrey, S.S., et al. (2005). A streamlined platform for high-content functional proteomics of primary human specimens. Nat. Methods *2*, 691–697.

Karlsson, M., Contreras, J.A., Hellman, U., Tornqvist, H., and Holm, C. (1997). cDNA cloning, tissue distribution, and identification of the catalytic triad of monoglyceride lipase. Evolutionary relationship to esterases, lysophospholipases, and haloperoxidases. J. Biol. Chem. *272*, 27218–27223.

Karlsson, M., Reue, K., Xia, Y.R., Lusis, A.J., Langin, D., Tornqvist, H., and Holm, C. (2001). Exon-intron organization and chromosomal localization of the mouse monoglyceride lipase gene. Gene *272*, 11–18.

Ledent, C., Valverde, O., Cossu, G., Petitet, F., Aubert, J.F., Beslot, F., Bohme, G.A., Imperato, A., Pedrazzini, T., Roques, B.P., et al. (1999). Unresponsiveness to cannabinoids and reduced addictive effects of opiates in CB1 receptor knockout mice. Science *283*, 401–404.

Leung, D., Hardouin, C., Boger, D.L., and Cravatt, B.F. (2003). Discovering potent and selective reversible inhibitors of enzymes in complex proteomes. Nat. Biotechnol. *21*, 687–691.

Li, W., Blankman, J.L., and Cravatt, B.F. (2007). A functional proteomic strategy to discover inhibitors for uncharacterized hydrolases. J. Am. Chem. Soc. *129*, 9594–9595.

Lichtman, A.H., Sheikh, S.M., Loh, H.H., and Martin, B.R. (2001). Opioid and cannabinoid modulation of precipitated withdrawal in delta9-THC and morphine-dependent mice. J. Pharmacol. Exp. Ther. *298*, 1007–1014.

Liu, H., Sadygov, R.G., and Yates, J.R., 3rd. (2004). A model for random sampling and estimation of relative protein abundance in shotgun proteomics. Anal. Chem. *76*, 4193–4201.

Liu, Y., Patricelli, M.P., and Cravatt, B.F. (1999). Activity-based protein profiling: the serine hydrolases. Proc. Natl. Acad. Sci. USA *96*, 14694–14699.

Long, J.Z., Li, W., Booker, L., Burston, J.J., Kinsey, S.G., Schlosburg, J.E., Pavon, F.J., Serrano, A.M., Selley, D.E., Parsons, L.H., et al. (2009). Selective blockade of 2-arachidonoylglycerol hydrolysis produces cannabinoid behavioral effects. Nat. Chem. Biol. *5*, 37–44.

Mackie, K. (2005). Distribution of cannabinoid receptors in the central and peripheral nervous system. Handb. Exp. Pharmacol. *168*, 299–325.

Mackie, K. (2006). Cannabinoid receptors as therapeutic targets. Annu. Rev. Pharmacol. Toxicol. *46*, 101–122.

Matsuda, L.A., Lolait, S.J., Brownstein, M.J., Young, A.C., and Bonner, T.I. (1990). Structure of a cannabinoid receptor and functional expression of the cloned cDNA. Nature *346*, 561–564.

Mechoulam, R., Ben-Shabat, S., Hanus, L., Ligumsky, M., Kaminski, N.E., Schatz, A.R., Gopher, A., Almog, S., Martin, B.R., Compton, D.R., et al. (1995). Identification of an endogenous 2-monoglyceride, present in canine gut, that binds to cannabinoid receptors. Biochem. Pharmacol. *50*, 83–90.

Motaghedi, R., and McGraw, T.E. (2008). The CB1 endocannabinoid system modulates adipocyte insulin sensitivity. Obesity (Silver Spring) *16*, 1727–1734.

Munro, S., Thomas, K.L., and Abu-Shaar, M. (1993). Molecular characterization of a peripheral receptor for cannabinoids. Nature *365*, 61–65.

Nomura, D.K., Blankman, J.L., Simon, G.M., Fujioka, K., Issa, R.S., Ward, A.M., Cravatt, B.F., and Casida, J.E. (2008a). Activation of the endocannabinoid system by organophosphorus nerve agents. Nat. Chem. Biol. *4*, 373–378.

Nomura, D.K., Hudak, C.S., Ward, A.M., Burston, J.J., Issa, R.S., Fisher, K.J., Abood, M.E., Wiley, J.L., Lichtman, A.H., and Casida, J.E. (2008b). Monoacylglycerol lipase regulates 2-arachidonoylglycerol action and arachidonic acid levels. Bioorg. Med. Chem. Lett. *18*, 5875–5878.

Okazaki, H., Igarashi, M., Nishi, M., Tajima, M., Sekiya, M., Okazaki, S., Yahagi, N., Ohashi, K., Tsukamoto, K., Amemiya-Kudo, M., et al. (2006). Identification of a novel member of the carboxylesterase family that hydrolyzes triacylglycerol: a potential role in adipocyte lipolysis. Diabetes *55*, 2091–2097.

Osei-Hyiaman, D., Liu, J., Zhou, L., Godlewski, G., Harvey-White, J., Jeong, W.I., Batkai, S., Marsicano, G., Lutz, B., Buettner, C., et al. (2008). Hepatic CB1 receptor is required for development of diet-induced steatosis, dyslipidemia, and insulin and leptin resistance in mice. J. Clin. Invest. *118*, 3160–3169.

Osuga, J., Ishibashi, S., Oka, T., Yagyu, H., Tozawa, R., Fujimoto, A., Shionoiri, F., Yahagi, N., Kraemer, F.B., Tsutsumi, O., et al. (2000). Targeted disruption of hormone-sensitive lipase results in male sterility and adipocyte hypertrophy, but not in obesity. Proc. Natl. Acad. Sci. USA *97*, 787–792.

Patricelli, M.P., Giang, D.K., Stamp, L.M., and Burbaum, J.J. (2001). Direct visualization of serine hydrolase activities in complex proteomes using fluorescent active site-directed probes. Proteomics *1*, 1067–1071.

Sugiura, T., Kondo, S., Sukagawa, A., Nakane, S., Shinoda, A., Itoh, K., Yamashita, A., and Waku, K. (1995). 2-Arachidonoylglycerol: a possible endogenous cannabinoid receptor ligand in brain. Biochem. Biophys. Res. Commun. *215*, 89–97.

Tabb, D.L., McDonald, W.H., and Yates, J.R., 3rd. (2002). DTASelect and Contrast: tools for assembling and comparing protein identifications from shotgun proteomics. J. Proteome Res. *1*, 21–26.

Tornqvist, H., and Belfrage, P. (1976). Purification and some properties of a monoacylglycerol-hydrolyzing enzyme of rat adipose tissue. J. Biol. Chem. *251*, 813–819.

Verty, A.N., Singh, M.E., McGregor, I.S., and Mallet, P.E. (2003). The cannabinoid receptor antagonist SR 141716 attenuates overfeeding induced by systemic or intracranial morphine. Psychopharmacology (Berl.) *168*, 314–323.

Zhang, D., Saraf, A., Kolasa, T., Bhatia, P., Zheng, G.Z., Patel, M., Lannoye, G.S., Richardson, P., Stewart, A., Rogers, J.C., et al. (2007). Fatty acid amide hydrolase inhibitors display broad selectivity and inhibit multiple carboxylesterases as off-targets. Neuropharmacology *52*, 1095–1105.

Zimmer, A., Zimmer, A.M., Hohmann, A.G., Herkenham, M., and Bonner, T.I. (1999). Increased mortality, hypoactivity, and hypoalgesia in cannabinoid CB1 receptor knockout mice. Proc. Natl. Acad. Sci. USA *96*, 5780–5785.